Bioorganic & Medicinal Chemistry 19 (2011) 1062–1071

Contents lists available at ScienceDirect

Bioorganic & Medicinal Chemistry

journal homepage: www.elsevier.com/locate/bmc

Collagen targeting using multivalent protein-functionalized dendrimers

Monica Breurken, Edith H. M. Lempens, Rinske P. Temming, Brett A. Helms [†], E. W. Meijer, Maarten Merkx [*]

Laboratory of Chemical Biology, Department of Biomedical Engineering, Eindhoven University of Technology, PO Box 513, 5600 MB Eindhoven, The Netherlands

ARTICLE INFO

Article history:
Available online 30 July 2010

Keywords:
Dendrimers
Multivalency
Collagen
Molecular imaging

ABSTRACT

Collagen is an attractive marker for tissue remodeling in a variety of common disease processes. Here we report the preparation of protein dendrimers as multivalent collagen targeting ligands by native chemical ligation of the collagen binding protein CNA35 to cysteine-functionalized dendritic divalent (AB_2) and tetravalent (AB_4) wedges. The binding of these multivalent protein constructs was studied on collagen-immobilized chip surfaces as well as to native collagen in rat intestinal tissues. To understand the importance of target density we also created collagen-mimicking surfaces by immobilizing synthetic collagen triple helical peptides at various densities on a chip surface. Multivalent display of a weak-binding variant (CNA35-Y175K) resulted in a large increase in collagen affinity, effectively restoring the collagen imaging capacities for the AB_4 system. In addition, dissociation of these multivalent CNA35 dendrimers from collagen surfaces was found to be strongly attenuated.

1. Introduction

Understanding and controlling the affinity and specificity of biomolecular recognition processes are of key importance to many areas of life sciences including targeted drug delivery, molecular imaging, and diagnostics.[1,2] Targeted nanoparticles such as quantum dots, liposomes, micelles, dendrimers, peptide nanotubes, etc. have gained wide popularity, both as drug delivery systems and as sensitive probes for molecular imaging.[3,4] A potentially useful property of nanoparticle-based targeting is that their size allows them to interact with complex biomolecular architectures using multiple weak interactions.[5] Such multivalent interactions can have profound effects on thermodynamic properties such as affinity and specificity, but also strongly attenuate dissociation kinetics.[6,7] At present, most insight into these effects has been obtained using well-defined model systems such as surfaces functionalized with synthetic receptor molecules.[8–10] In contrast, few experimental studies have addressed these questions for biomedically relevant multivalent targets.[11] This is particularly true for protein-functionalized nanoparticles, where a lack of efficient and chemoselective conjugation methods has hampered the synthesis of nanoparticles with a defined valency of active protein ligands.[12–16]

Because of their abundance, accessibility and repetitive structure, extracellular matrix (ECM) proteins provide attractive targets for multivalent targeting. Collagen in particular is an important marker for the many diseases that are characterized by remodeling of the extracellular matrix. Examples of these include the process of angiogenesis in cancer, the formation of scar tissue following myocardial infarction and the distinction between stable and vulnerable plaques in atherosclerosis.[17–20] Collagen, like many structural ECM proteins, is characterized by a highly repetitive structure and a complex 3D organization. Its primary sequence consists of a characteristic Gly-X-Y repeat, where the X and Y positions are often occupied by a proline (P) and hydroxyproline (O).[19,21,22] The presence of a glycine residue at every third position allows the formation of a characteristic right-handed triple helix, a structure common to all 26 different collagen families. Through a combination of self-assembly and covalent cross-linking, these collagen triple helices subsequently organize into a wide variety of complex 3D architectures ranging from fibrils and fibers to networks. Given the repetitive nature of the collagen sequence and its modular architecture, it is not surprising that multivalency plays an important role in many natural interactions of collagen.[23,24]

Two recent examples from our group illustrate the potential of semi-synthetic multivalent ligands to target collagen with high affinity and specificity. In one approach peptide phage display was used to identify linear 7-mer peptides with a moderate affinity for collagen type I.[25] Multivalent display of this peptide on a pentavalent dendritic AB_5 scaffold was shown to successfully mimic the multivalent architecture of the peptides displayed on the original phage, resulting in a 100-fold increase in collagen affinity. Another demonstration of the potency of multivalent interactions was provided by a second study that used micelles and liposomes as multivalent scaffolds for the collagen binding protein CNA35.[14,25] This well-characterized collagen binding protein binds various types of collagen with a K_d of 0.5 μM by wrapping around the collagen triple helix[26] and was shown to be a useful probe to monitor collagen formation in tissue engineering and in atherosclerotic plaques.[27,28] Multivalent binding of CNA35-micelles was shown to dramatically

* Corresponding author. Fax: +31 402451036.
E-mail address: m.merkx@tue.nl (M. Merkx).
† Present address: The Molecular Foundry, Lawrence Berkeley National Laboratory, One Cyclotron Road, MS 67R6110, Berkeley, USA.

0968-0896/$ - see front matter © 2010 Elsevier Ltd. All rights reserved.
doi:10.1016/j.bmc.2010.07.058

decrease the dissociation rate of these micelles in surface plasmon resonance binding (SPR) studies, being stable for more than 8 h under conditions of continuous flow. Moreover, micelles and liposomes functionalized with multiple copies of a so-called 'non-binding' variant of CNA35[29] containing a Y175K point mutation in the collagen binding site, showed a remarkable enhancement of the binding affinity, effectively restoring the collagen imaging properties of fluorescently labeled micelles.

Liposomes and micelles are attractive molecular imaging nanoparticles because of their ease of synthesis and their ability to carry large payloads,[30] but their relatively large size may prevent penetration in dense tissues such as the ECM. In addition, recent studies have shown that protein–lipid exchange in these protein-functionalized micelles is quite fast at 37 °C.[31] Here we report the preparation of protein dendrimers as multivalent collagen targeting ligands by coupling wt-CNA35 and CNA35-Y175K to cysteine-functionalized dendritic divalent (AB_2) and tetravalent (AB_4) wedges. In addition to providing more compact, well-defined multivalent ligands, the availability of these protein dendrimers allowed us to investigate in more detail the critical design elements for effective multivalent targeting of collagen. To better understand the importance of target density we not only studied the interaction of these CNA35-dendrimers with native collagen, but also created collagen-mimicking surfaces by immobilizing synthetic collagen triple helical peptides at various densities on a biosensor chip surface.

2. Results and discussion

2.1. Synthesis of multivalent dendritic wedges functionalized with CNA35

The AB_x-type of dendritic wedges used in this study were previously shown to provide a versatile platform for the synthesis of multivalent peptide ligands with control over valency (x), spacer length and the presence of a bioorthogonal reactive functionality (A) for further bioconjugation.[32,33] While efficient native chemical ligation (NCL) between the cysteines present at the ends of the PEG-arms was observed for a variety of peptide thioesters, functionalization with recombinant protein domains had previously not been shown. In fact, in a previous study we observed that native chemical ligation of GFP-MESNA to a 1st generation cysteine-functionalized poly(propylene imine) (PPI) dendrimer resulted in a mixture of 1, 2, 3, and 4-times ligated products.[15] CNA35 and CNA35-Y175K with C-terminal MESNA thioesters were obtained using the IMPACT system as described before.[25] To push the reaction of CNA35-MESNA with the cysteine-functionalized wedges to completion as much as possible, an eightfold molar excess of CNA35-MESNA was incubated overnight with AB_2 and AB_4, respectively (Scheme 1). In addition, the reaction was performed in the presence of (4-carboxylmethyl) thiophenol (MPAA), an improved catalyst for NCL reported by Johnson and Kent[34] that was also used successfully in the preparation of multivalent CNA35 micelles and liposomes.

SDS–PAGE analysis of the ligation to the AB_2 wedge showed efficient formation of the CNA35-dimer, as indicated by the presence of a band at 70 kDa (see Supplementary data, Fig. S1). Most of the unreacted CNA35 could be removed using size exclusion chromatography (SEC), although a small contamination of monomeric CNA35 remained present even after repeated chromatography steps (Fig. 1A). Ligation reactions using the AB_4 wedge under similar conditions yielded two ligation products, with bands at apparent molecular weight of 200 kDa and 260 kDa (see Supplementary data, Fig. S1). These bands were attributed to the three and four times ligated species, respectively. Their branched structure causes the bands of $(CNA35)_3$ and $(CNA35)_4$ to appear at a higher apparent molecular weight, a phenomenon that was observed before for multivalent GFP constructs.[15] Although NCL to

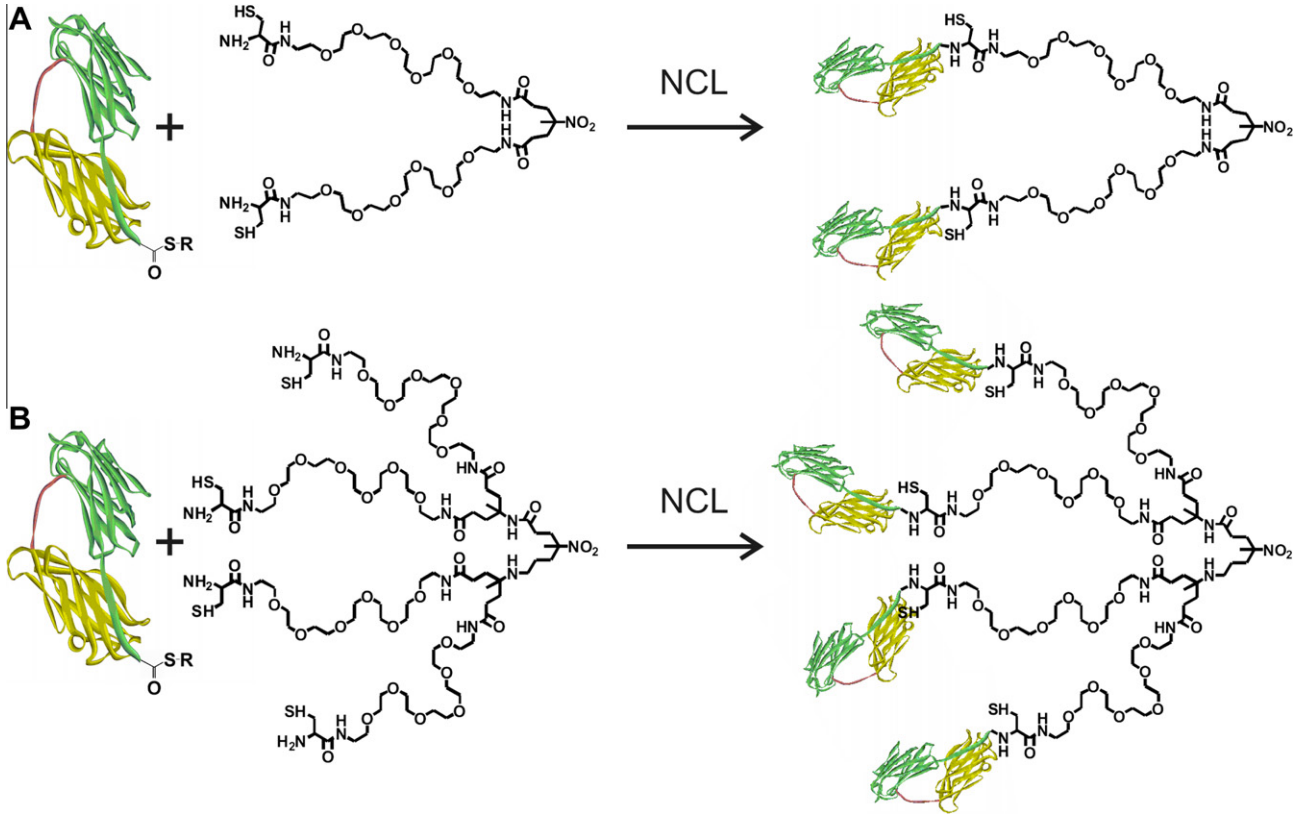

Scheme 1. Synthesis of divalent (A) and tetravalent (B) CNA35 dendrimers by native chemical ligation (NCL) of CNA35-MESNA to AB_2 and AB_4 cysteine-functionalized dendritic wedges.

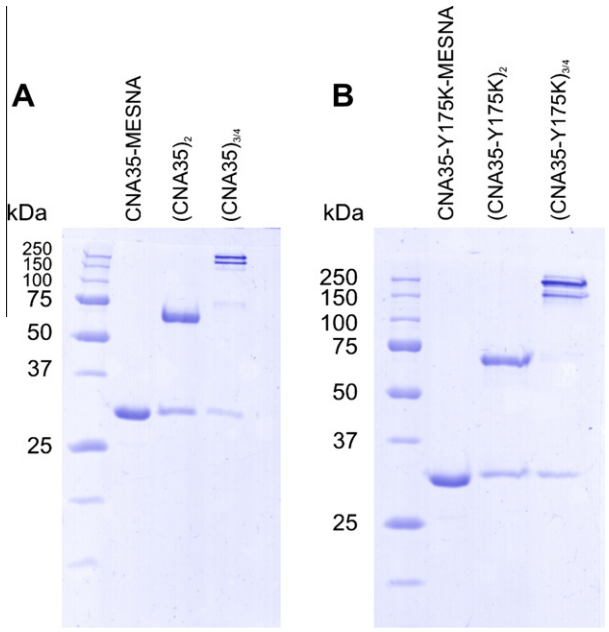

Figure 1. SDS–PAGE (12%) analysis of purified multivalent dendrimers displaying (A) wt CNA25 or (B) CNA35-Y175K.

the AB_4 wedge did not result in complete conversion, these results nonetheless represent a clear improvement over the previously reported synthesis of GFP dendrimers, which resulted in a distribution of 1, 2, 3, and 4-times ligated products. Unfortunately, the relatively small difference in volume between $(CNA35)_3$ and $(CNA35)_4$ prevented the separation of these species using size exclusion chromatography. We therefore decided to continue our studies using this mixture of trivalent and tetravalent CNA35 (denoted as $(CNA35)_{3-4}$) and compare its collagen targeting properties with those of monovalent CNA35 and divalent $(CNA35)_2$ (Fig. 1).

2.2. Binding of multivalent CNA35 ligands to human collagen type I studied using SPR

Because SPR allows direct real-time monitoring of protein binding to protein-functionalized surfaces, this technique is ideally suited to study the kinetics of multivalent interactions with complex biomacromolecules such as collagen. Figure 2A shows the association and dissociation of monovalent CNA35, $(CNA35)_2$, and $(CNA35)_{3-4}$ to an SPR chip surface functionalized with 1500 RU of human collagen type I. All binding experiments were performed at a concentration of 0.5 μM[‡] CNA35 domain, which corresponds to the apparent K_D of monovalent CNA35.[35] Previous SPR studies of CNA35 binding to collagen showed a complex binding behavior and the presence of a variety of high and low affinity binding sites, which were attributed to the heterogeneous nature of native collagen.[36,37] The SPR trace for monovalent CNA35 also reveals at least two different binding sites, which is most apparent in the dissociation curve that cannot be fit using a single exponential function consistent with the presence of multiple kinetic phases. This heterogeneity prevents the accurate determination of K_d-values, but comparison of the SPR traces for the various CNA35 ligands still provides useful qualitative insights. An increase in response level is observed for the multivalent structures in comparison to CNA35-MESNA, but a significant part of this increase can simply be attributed to the higher molecular weight of the multivalent constructs. A more interesting difference is the clear decrease in dissociation rate that is observed upon increasing the ligand valency, which is a signature of multivalent interactions. In fact, most of $(CNA35)_{3-4}$ stays associated with the collagen even after 8 h of continuously flowing buffer over the chip surface (Fig. 3). This enhanced stability was also observed previously for multivalent CNA35-micelles,[25] showing that this is an intrinsic property of multivalent CNA35 ligands that is independent of the nature of the multivalent scaffold.

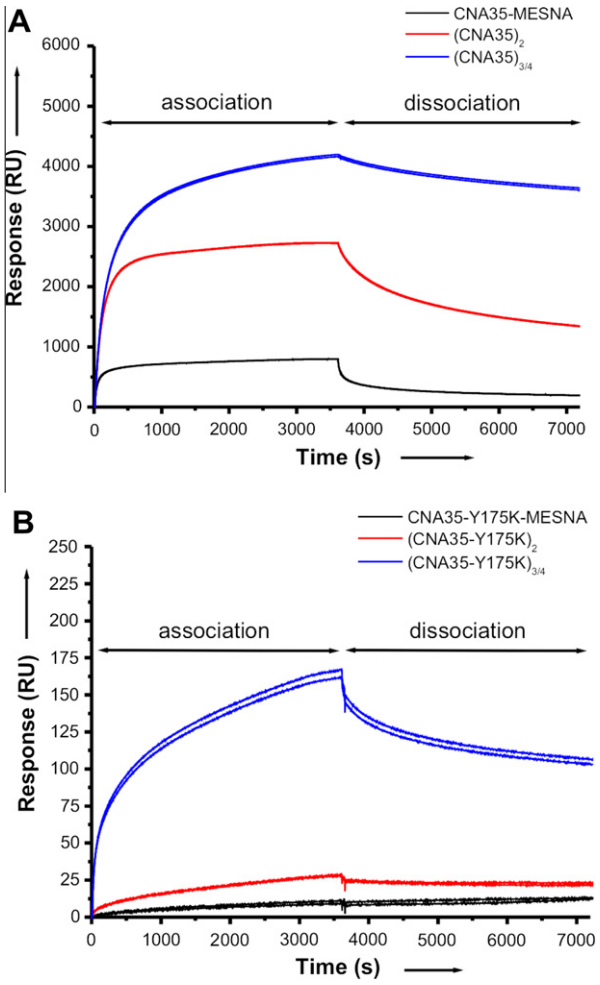

Figure 2. SPR analysis of the binding of multivalent CNA35 ligands to human collagen type I. A CM5 chip was functionalized with human collagen type I (1506 RU bound). Proteins were flown over the chip for 60 min at a protein concentration of 0.5 μM followed by 60 min of dissociation using 10 mM HBS pH 7.4 containing 1 mg/mL bovine serum albumin (BSA). Duplicate traces are shown for each experimental condition.

A more pronounced effect of ligand valency was observed for the constructs bearing the weakly-binding CNA35-Y175K mutant (Fig. 2B). Here, a large increase in binding level was observed between the $(CNA35\text{-}Y175K)_2$ and $(CNA35\text{-}Y175K)_{3-4}$. These results are consistent with previous results obtained for multivalent CNA35-micelles, which showed a substantial increase in collagen binding level between micelles displaying on average one and five copies of CNA35-Y175K per micelle.[25] In fact, the results obtained for the CNA35-dendrimers imply the presence of a 'threshold' of at least 3 interactions that are necessary to 'restore' the collagen binding affinity of CNA35-Y175K for native collagen. The lower level of response units for $(CNA35\text{-}Y175K)_{3-4}$ compared to $(CNA35)_{3-4}$ most likely reflects the limited number of binding sites on collagen that allow these tri- or tetravalent interactions.

[‡] Please note that this is the concentration of CNA35, not the concentration of the complete molecule.

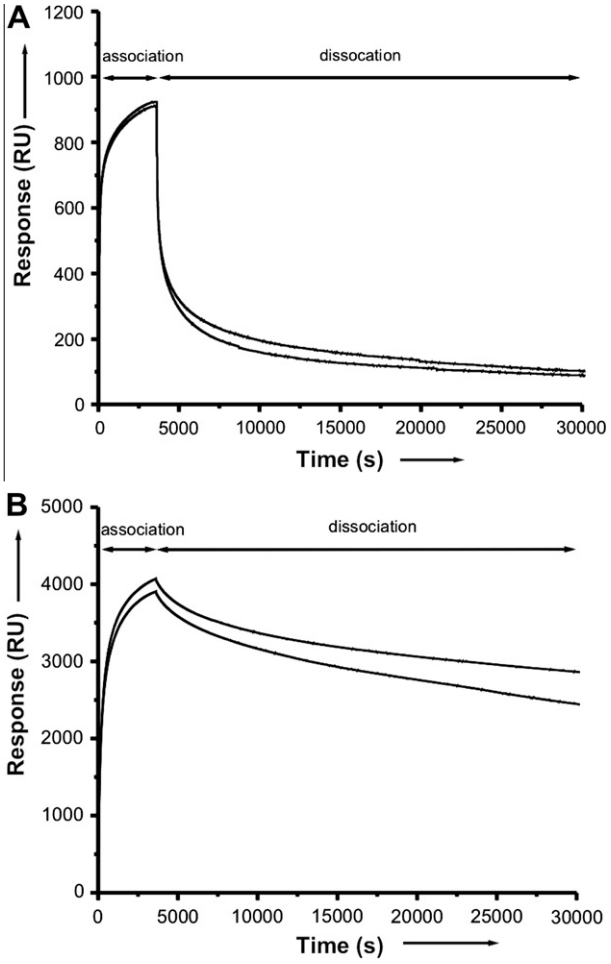

Figure 3. SPR analysis of binding of (A) CNA35-MESNA and (B) $(CNA35)_{3-4}$-AB_4 to human collagen type I. A CM5 chip was functionalized with human collagen type I (1506 RU bound). Proteins were flown over the chip at 25 °C for 60 min at a protein concentration of 0.5 μM followed by 8 h of dissociation. 10 mM HBS pH 7.4 containing 1 mg/mL BSA was used as a running buffer. Duplicate traces are shown for each experimental condition.

2.3. Multivalent binding to surfaces with a tunable density of synthetic collagen peptides

Native collagen is a very complex biomolecular target that is organized at different hierarchical levels (fibrils, fibers) and displays substantial heterogeneity due to, amongst other possibilities, differences in cross linking.[21] To better understand the importance of target density we not only studied the interaction of these CNA35-dendrimers with native collagen, but also synthesized short synthetic collagen triple helical peptides for immobilization on the SPR chip surfaces. The use of synthetic collagen mimics provides a much more homogenous type of CNA35 binding site, and in addition presents an opportunity to tune the density of CNA35-binding sites and thus to study the role of target valency on the binding properties of multivalent CNA35 ligands. Various groups have reported template-assisted methods to stabilize the formation of small collagen triple helices from short collagen peptide repeats. For example, Feng et al. showed that the melting temperature of $(GPO)_5$ increases from 18 °C to 70 °C after coupling 3 copies of this peptide to Kemp's triacid.[38] Here, we used a similar template-based approach to arrive at a collagen mimic that is very stable and can be used as a soluble form of collagen that provides a single CNA35 binding site for use in SPR binding experiments.

A trivalent AB_3 dendritic wedge similar to the ones used in multivalent ligands synthesis was synthesized to serve as a scaffold for the triple helix forming peptides (Scheme 2). Briefly, an orthogonal protecting group strategy was used to introduce a glycine at the focal point of commercially available aminotriester (**1**). The additional spacing allowed efficient subsequent conjugation to carboxymethyl groups present on the BIAcore chip. Polyethylene glycol units functionalized with acid-labile tBoc-protected amino-oxy groups (**5**) were coupled to the activated periphery of the dendron. After deprotection, three glyoxyl-functionalized peptides containing five repeats of glycine (G), proline (P) and 4-hydroxyproline (O; $(GPO)_5$) were coupled to the amino-oxy end groups via oxime ligation (**9**). Formation of a collagen triple helix was confirmed by circular dichroism (CD) measurements in H_2O, which showed a small positive peak at 225 nm and a large negative peak at 200 nm, both of which are characteristic for the triple helical conformation. Temperature dependent CD measurements revealed reversible melting of the triple helix at 55 °C, while no triple helix formation was observed for the non-templated $(GPO)_5$ peptide at RT (see Supplementary data, Fig. S2).

Binding of wt CNA35 to an SPR chip functionalized with ~50 RU of the collagen mimic showed fast association and dissociation kinetics consistent with a classical bimolecular interaction. Plotting the steady-state levels of bound CNA35 as a function of CNA35 concentration revealed a K_d of 2 μM, which is similar to the (average) affinity of CNA35 to native collagen[35–37] (Fig. 4). Next, SPR chips with three different levels of immobilization (~5 RU, ~200 RU, ~900 RU) were obtained to test the influence of surface density on multivalent interactions. Binding of monovalent CNA35-MESNA to the low density chip (5 RU) shows fast association and dissociation behavior. $(CNA35)_2$ and $(CNA35)_{3-4}$ also show fast association kinetics, but both multivalent ligands show biphasic dissociation kinetics (Fig. 5). The fast component, which we attribute to monovalent binding, dominates the dissociation behavior of $(CNA35)_2$ and is also the major component for $(CNA35)_{3-4}$. At higher immobilization levels, an increase in the relative contribution of the slow component in the dissociation kinetics becomes apparent, indicating an increased match between the multivalent ligands and their target. It may be surprising that even at the low level of immobilization, some multivalent binding is observed in case of $(CNA35)_{3-4}$. However, the 5 RU of immobilized collagen mimic (5 pg/mm^2) corresponds to a 'concentration' of ~9 μM collagen binding sites in the dextran layer covering the SPR chip.

The remarkable difference in binding efficiency between divalent and tri/tetravalent CNA35-Y175K that was observed for native collagen type I, is also observed for these synthetic collagen-mimicking surfaces (Fig. 6). No binding was observed for both the monovalent and divalent CNA35-Y175K ligands for any of the three different densities, whereas $(CNA35\text{-}Y175K)_{3-4}$ shows significant binding in all cases, in particular with the 200 and 900 RU chips. The slow apparent association rate for $(CNA35\text{-}Y175K)_{3-4}$ compared to $(CNA35)_{3-4}$ may be explained by the fact that binding of $(CNA35\text{-}Y175K)_{3-4}$ requires the formation of three simultaneous interactions, whereas for binding of $(CNA35)_{3-4}$ only a single interaction is sufficient. These observations thus further strengthen a model in which at least three simultaneous interactions are required in order to get efficient binding of CNA35-Y175K variants to collagen.

2.4. Imaging collagen in native tissue

To establish the performance of multivalent CNA35 dendrimers in native tissue, we compared the collagen imaging properties of monovalent wt CNA35 and CNA35-Y175K with their two multivalent counterparts, $(CNA35)_{3-4}$ and $(CNA35\text{-}Y175K)_{3-4}$ using slices

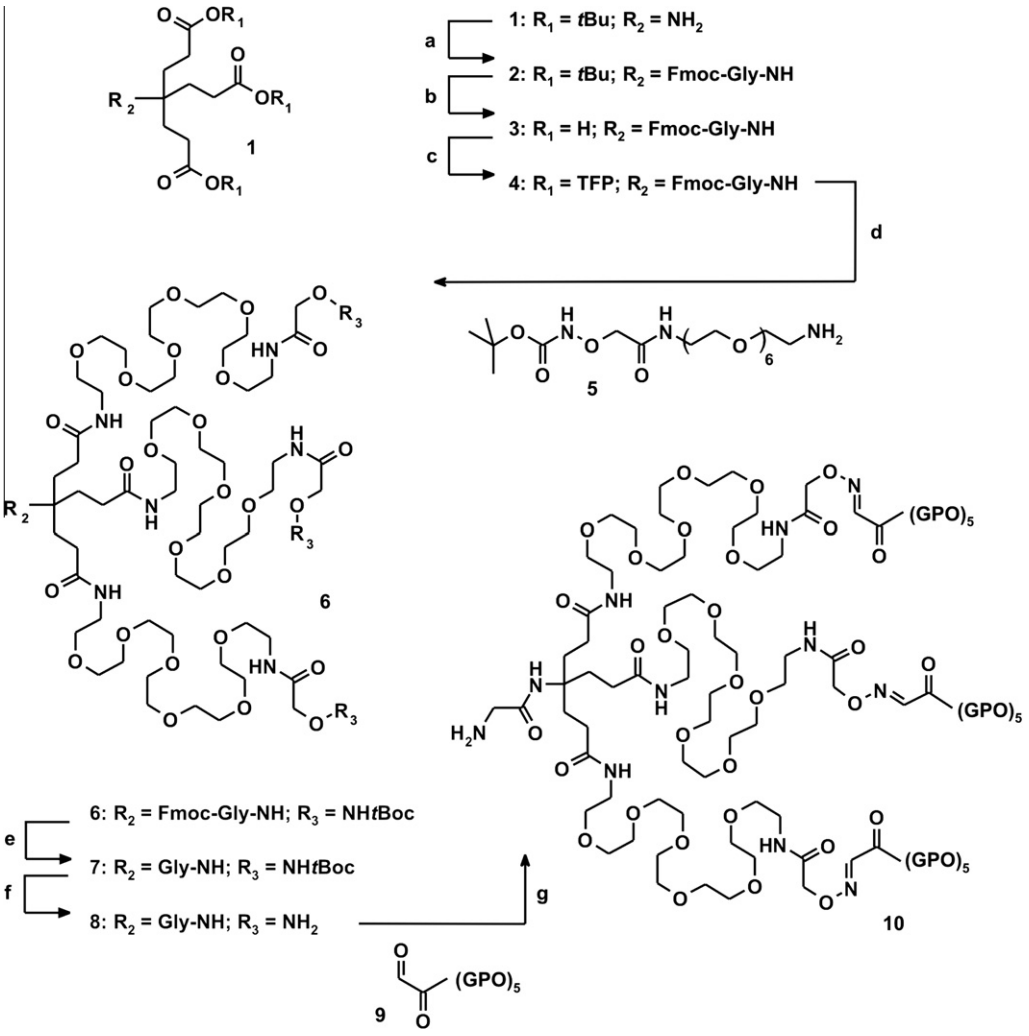

Scheme 2. Synthesis of a synthetic collagen mimic. (a) Fmoc-Gly-OH, 2-(1H-7-azabenzotriazol-1-yl)-1,1,3,3-tetramethyl uronium hexafluorophosphate (HATU), DIPEA, DCM. (b) HCO_2H. (c) 2,3,5,6-Tetrafluorophenol (TFP), pyridinium *para*-toluenesulfonate (PPTS), *N*,*N*′-dicyclohexylcarbodiimide (DCC), DCM. (d) DIPEA, DCM. (e) 20% piperidine in DCM. (f) Trifluoroacetic acid (TFA), triisopropylsilane, H_2O. (g) Glyoxyl-$(GPO)_5$, 10 mM sodium phosphate buffer pH 6.5.

of rat intestinal tissue. The CNA35 proteins were labeled with Oregon Green 488 succinimide yielding a degree of labeling of 2.6–2.9 per protein domain. This labeling procedure primarily affects lysine residues at the protein's C-terminus and was previously shown to not interfere with collagen binding.[39] Figure 7 shows images obtained using confocal fluorescence microscopy of rat intestinal tissue samples that were incubated with these probes at a protein concentration of 0.5 μM.[§] The observed structures are collagen fibers present in the basement membrane lining the intestinal epithelial cells.[29] Within them substructures can be distinguished, which we assign to capillaries in the intestinal villi. Although somewhat higher fluorescence intensity was expected for the multivalent construct, no significant difference in the intensity or staining pattern was observed between monovalent CNA35 and $(CNA35)_{3-4}$. Tissue-to-tissue variation makes it difficult to reliably distinguish relatively small differences in binding levels, however. In addition, it could be that in native tissues binding of the multivalent constructs is somewhat limited by their larger size compared to monovalent CNA35. A marked difference between monovalent and multivalent ligands was observed for the CNA35-Y175K variant. Whereas hardly any staining was observed for monovalent CNA35-Y175K, again a remarkable 'restoration' of collagen targeting was observed for the dendritic wedge presenting 3–4 copies of this weakly binding CNA35 variant.

3. Conclusion

Semi-synthetic multivalent collagen binding proteins were obtained by native chemical ligation of CNA35-thioesters and cysteine-functionalized AB_2 and AB_4 dendritic wedges. While ligation of the latter did not go to completion, as far as we know these protein dendrimers still represent the first examples of multivalent targeting ligands based on covalent coupling of a recombinant protein and a synthetic dendritic scaffold. Compared to the previously reported micelles and liposomes, these protein dendrimers offer increased stability and smaller size. The multivalent CNA35 dendrimers recapitulate many of the remarkable collagen binding properties previously observed for CNA35 micelles, including a strong attenuation of dissociation kinetics and the ability to enhance the affinity of 'non-binding' collagen binding protein (CNA35-Y175K). Binding studies using both native collagen and surfaces functionalized with various densities of synthetic collagen triple helical peptides revealed that this 'restoration' of collagen affinity required the presence of at least

[§] Please note that this is the concentration of CNA35, not the concentration of the complete molecule.

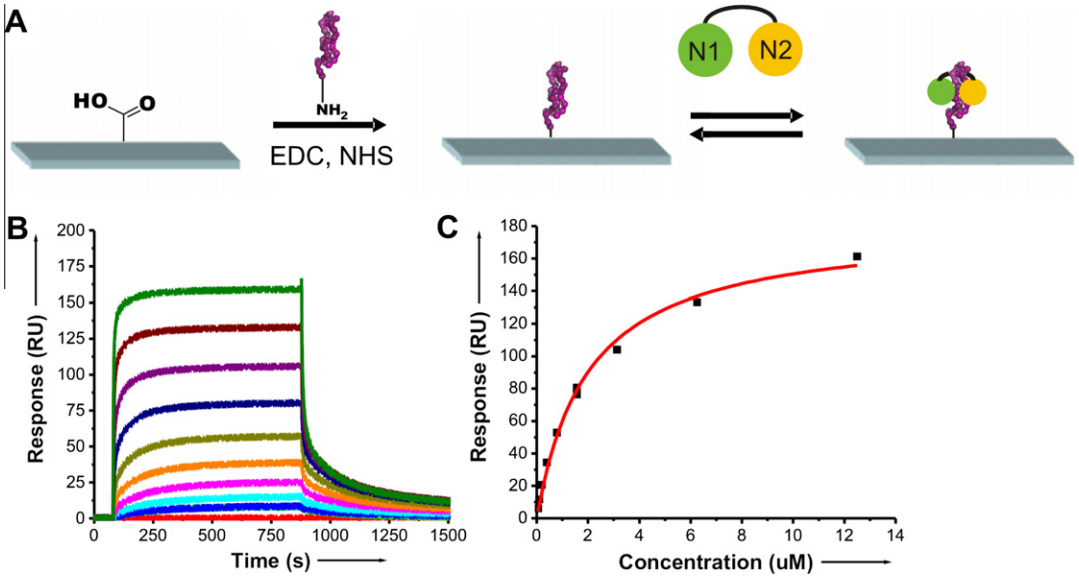

Figure 4. Affinity measurements of CNA35 binding to a collagen mimic immobilized on an SPR chip. (A) Immobilization of collagen mimic on the SPR chip via amine coupling allows analysis of interaction between CNA35 and a single well-defined binding site. (B) SPR analysis of binding of wt CNA35 to the collagen mimic at different concentrations ranging from 49 nM to 12.5 μM. A CM5 chip was functionalized with the collagen mimic (50 RU bound). (C) Response levels at equilibrium as a function of CNA35 concentration. The solid line reflects the best fit using a 1:1 single site binding model yielding a K_D of 2 μM.

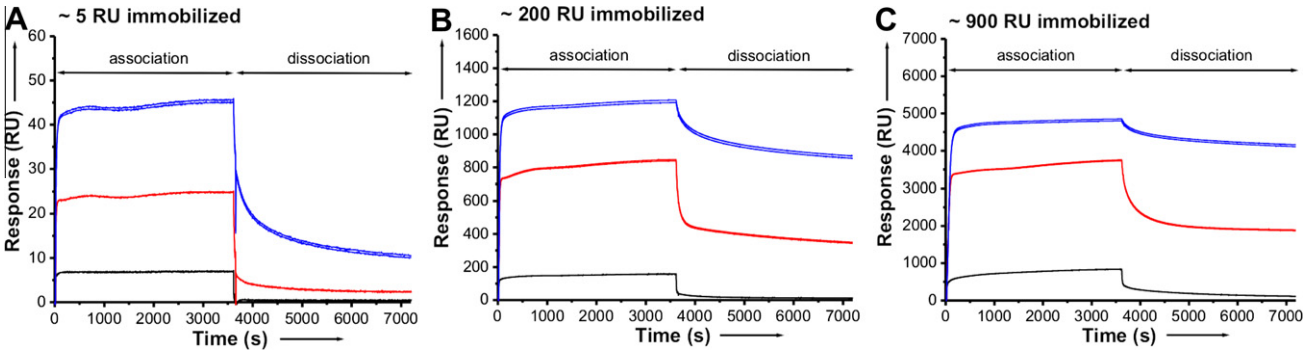

Figure 5. SPR analysis of binding of CNA35-MESNA (black lines), $(CNA35)_2$ (red lines) and $(CNA35)_{3-4}$ (blue lines) to the collagen mimic. Proteins were flown over the chip at a protein concentration of 0.5 μM for 60 min, followed by 60 min of dissociation with (A) ~5 RU of collagen mimic immobilized, (B) ~200 RU of collagen mimic immobilized and (C) ~900 RU immobilized. Duplicate traces are shown for each experimental condition.

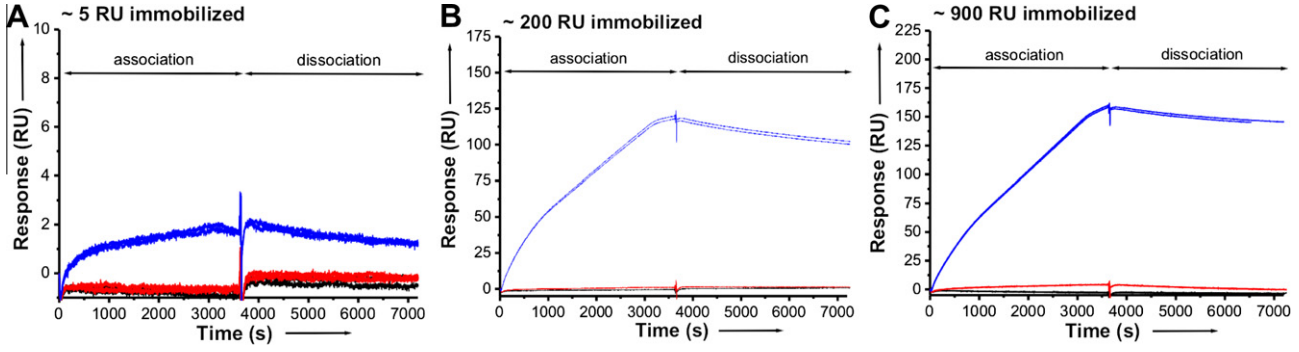

Figure 6. SPR analysis of binding of CNA35-Y175K-MESNA (black lines), $(CNA35\text{-}Y175K)_2$ (red lines) and $(CNA35\text{-}Y175K)_{3-4}$ (blue lines) to the collagen mimic. Proteins were flown over the chip at a protein concentration of 0.5 μM for 60 min, followed by 60 min of dissociation with (A) ~5 RU of collagen mimic immobilized, (B) ~200 RU of collagen mimic immobilized and (C) ~900 RU immobilized. Duplicate traces are shown for each experimental condition.

three simultaneous interactions. The results obtained in this study illustrate the strength of using multiple weak interactions to increase targeting to multivalent architectures such as collagen, but also provide a warning when interpreting the results of control experiments using nanoparticles functionalized with 'non-binding' targeting proteins.

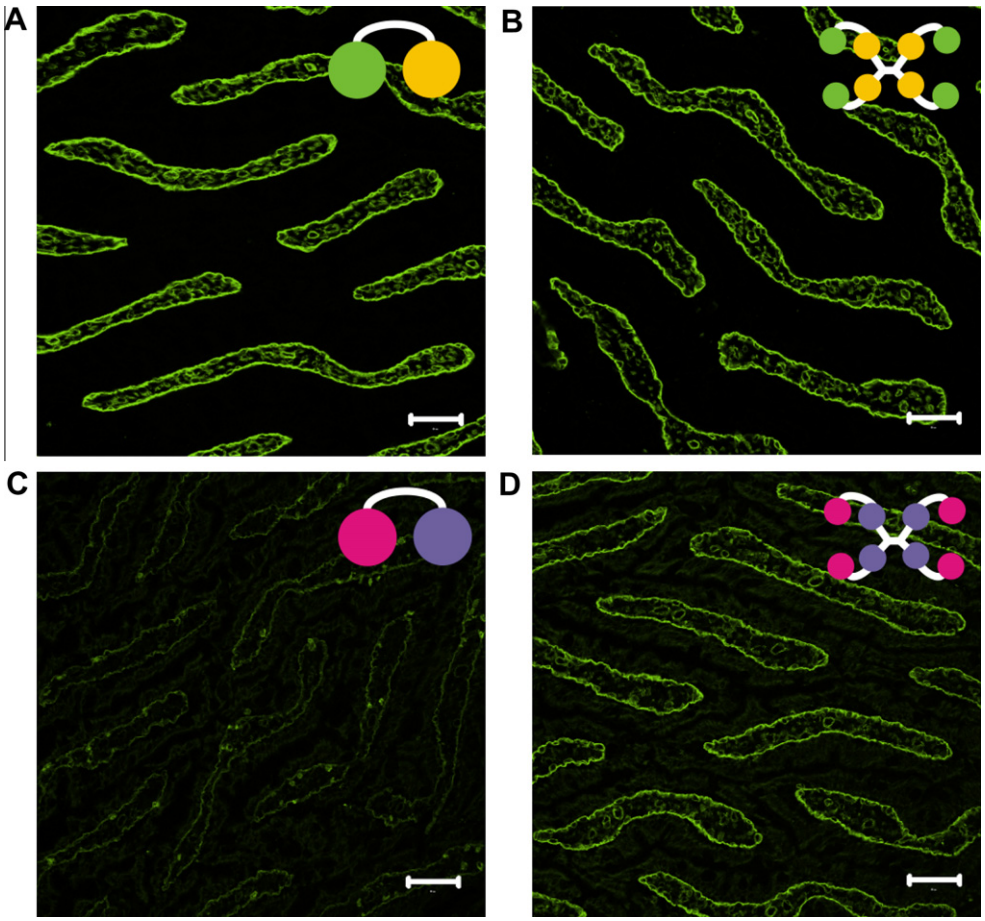

Figure 7. Confocal fluorescence microscopy image of rat intestinal tissue after overnight incubation with fluorescently labeled CNA35 (A), $(CNA35)_{3-4}$ (B), CNA35-Y175K (C) and $(CNA35\text{-}Y175K)_{3-4}$. (D). All experiments were done using 0.5 μM protein domains. Scale bar represents 50 μm.

4. Experimental section

4.1. General

Unless stated otherwise, all reagents and chemicals were commercially obtained and used without any further purification. (4-carboxylmethyl) thiophenol (MPAA), tris(2-carboxyethyl) phosphine hydrochloride (TCEP) and human collagen type I from human placenta (C7774) were purchased from Sigma. Oregon Green 488 NHS ester (O-6147) was obtained from Invitrogen. UV–vis spectra were recorded on a NanoDrop ND-1000 Spectrophotometer (Thermo Scientific). Primers were purchased from MWG (Ebersberg, Germany). For the synthesis of the collagen mimic, ^{1}H and ^{13}C NMR spectra were acquired on a Varian 400-MR spectrometer at 400 and 100 MHz, respectively, in deuterated solvents containing 0.5% v/v TMS; chemical shifts are listed in ppm relative to TMS as an internal standard. ESI-MS spectra were recorded on an Applied Biosystems Single Quadrupole Electrospray Ionization Mass Spectrometer API-150EX in positive mode. MALDI-TOF mass spectrometry has been performed using a PerSeptive Biosystems Voyager DE PRO Spectrometer. Reversed phase HPLC was performed on a Shimadzu LC-8A HPLC system by using a Vydac C18 column. A gradient of acetonitrile in water, both containing 0.1% TFA was used to elute the compounds. Detection was performed by an UV-detector (λ = 214 nm). Peptide synthesis was performed on a Prelude automated peptide synthesizer (Protein Technologies) using standard Fmoc chemistry. All CD experiments were performed on a Jasco J-815 CD spectrometer equipped with a Jasco PTC-348 WI temperature controller. The spectra were obtained using a 1.0 mm Quartz cuvet with a scanning speed of 50 nm/min, a band width of 1 nm, and a response of 0.5 s. The temperature dependent spectra were obtained with a speed of 10 °C/h.

4.2. Protein expression and purification

CNA35, CNA35-MESNA, and CNA35-Y175K-MESNA were obtained as described previously.[25,32,35] The Y175K mutation was introduced in pQE30-CNA35 using the QuickChange Site-directed mutagenesis kit (Stratagene) using the primers: 5′-CGGGAACAAG TAGTGTTTTCTATAAAAAAACGGGAGATATGCTACC-3′ and 5′-GGTAG CCATATCTCCCGTTTTTTTATAGAAAACACTACTTGTTCCCG-3′ yielding pQE30-CNA35-Y175K. The correct sequence of the gene was confirmed by DNA sequencing (Baseclear). The expression plasmid was transformed into *Escherichia coli* Bl21 (DE3) cells and expressed as described previously.[35] The isolated proteins were directly applied to a column of 3 mL HisBind resin (Novagen) charged with $NiSO_4$. The column was washed with bind buffer (20 mM Tris, 0.5 mM NaCl, 5 mM imidazole, pH 7.9) followed by wash buffer (20 mM Tris, 0.5 mM NaCl, 15 mM imidazole, pH 7.9). Subsequently, the column was flushed with elution buffer (20 mM Tris, 0.5 mM NaCl, 1 M imidazole, pH 7.9). Imidazole was directly removed from the elution fraction and buffer was exchanged to HBS (10 mM Hepes, 135 mM NaCl, pH 7.4) by repeated concentration and dilution using an Amicon Ultra-4 centrifugal concentrator with a 10 kDa cut-off. The concentration of CNA35-Y175K was determined by UV–vis using ε_{280nm} = 29,910 M^{-1} cm^{-1}.

4.3. Preparation of multivalent CNA35 ligands

Both dendritic wedges AB_2 and AB_4 were synthesized as described before.[33] Native chemical ligation reactions were performed in 20 mM sodium phosphate, 500 mM NaCl, 50 mM MPAA and 2 mM TCEP at a protein concentration of ~450 μM. A four and eightfold molar excess CNA35 MESNA thioester was used for reactions with AB_2 and AB_4, respectively. The pH was adjusted to ~6.2 with 1 M sodium phosphate, pH 9.2. After overnight incubation at room temperature, the reaction mixture was buffer exchanged to HBS, pH 7.4 to remove MPAA and TCEP by repeated concentration and dilution using an Amicon Ultra-4 centrifugal concentrator with a 10 kDa cut-off. The reaction mixtures were purified using a Superdex 75 size exclusion column (GE Healthcare) connected to an ÅKTA FPLC system (GE Healthcare) using HBS as a running buffer at a flow rate of 0.8 mL/min.

4.4. Synthesis of the collagen mimic

4.4.1. Fmoc-Gly-(tBu)$_3$ (2)

Fmoc-Gly-OH (894 mg, 3.008 mmol) and DIPEA (1.213 g, 9.385 mmol) were dissolved in DMF (20 mL) before the addition of aminotriester (**1**) (1.000 g, 2.406 mmol). The mixture was cooled to 0 °C and HATU (1.189 g, 3.128 mmol) was subsequently added as a solid. After stirring for 17 h at room temperature, the solvent was evaporated under reduced pressure. DCM (100 mL) was added and the mixture was washed with an aqueous saturated $NaHCO_3$ solution (3 × 100 mL). After drying on $MgSO_4$ and concentration, the crude product was purified by flash chromatography (DCM, followed by DCM/MeOH; 98:2). The title compound was obtained as a white solid (1.442 g, 72%). ^{1}H NMR ($CDCl_3$, 200 MHz): δ 7.69 (d, 2H, J = 6.6 Hz); 7.53 (d, 2H, J = 6.6); 7.28 (m, 4H); 6.42 (s, 1H); 5.40 (br s, 1H); 4.34 (d, 2H, J = 7.0 Hz); 4.16 (t, 1H, J = 6.6 Hz); 3.73 (d, 2H, J = 4.3 Hz); 2.16 (t, 6H, J = 7.8 Hz); 1.91 (t, 6H, J = 7.4 Hz); 1.37 (s, 27H). ^{13}C NMR ($CDCl_3$, 50 MHz): δ 172.7; 169.0; 156.9; 144.4; 141.2; 128.1; 127.6; 125.8; 120.6; 80.1; 66.2; 57.1; 47.1; 43.8; 29.5; 28.2. IR (cm^{-1}): ν 3297, 2976, 1721, 1655, 1525, 1366, 1314, 1230, 1145, 1100, 1044, 848, 785, 738. MALDITOF-MS: calcd $C_{39}H_{54}N_2O_9Na^+$: m/z 717.56; found m/z 717.56.

4.4.2. Fmoc-Gly-(OH)$_3$ (3)

Fmoc-Gly-(tBu)$_3$ (**2**) (1.000 g, 1.504 mmol) was dissolved in formic acid (10 mL) and stirred for 8 h. Evaporation of formic acid under reduced pressure was followed by co-evaporation with toluene (3 × 25 mL). After drying in vacuo, the product was obtained (739 mg, 93%). ^{1}H NMR (DMSO-d_6, 400 MHz): δ 7.89 (d, 2H, J = 7.7 Hz); 7.71 (d,2H, J = 7.3 Hz) 7.41 (t, 2H, J = 7.1 Hz); 7.33 (t, 2H, J = 7.3 Hz); 4.28 (d, 2H, J = 6.2 Hz), 3.85 (s, 1H), 3.57 (d, 2H, J = 5.9 Hz); 2.13 (t, 6H, J = 7.9 Hz); 1.83 (t, 6H, J = 7.7 Hz). ^{13}C NMR (DMSO-d_6, 50 MHz): δ 174.5; 168.7; 156.6; 143.9; 141.8; 127.7; 127.1; 125.3; 120.2; 65.5; 56.4; 46.9; 43.5; 29.1; 28.0. IR (cm^{-1}): ν 3333, 2955, 1731, 1698, 1639, 1533, 1451, 1312, 1258, 1171, 1136, 1083, 1049, 933, 759, 741. MALDI-TOF-MS: calcd $C_{27}H_{30}N_2O_9Na^+$: m/z 549.18; found m/z 549.30.

4.4.3. Fmoc-Gly-(TFP)$_3$ (4)

2,3,5,6-Tetrafluorophenol (90 mg, 0.597 mmol), DMAP (7 mg, 0.054 mmol) and Fmoc-Gly-(OH)$_3$ (**3**) (95 mg, 0.181 mmol) were dissolved in dry DCM (2 mL). Subsequently, 1-(3-dimethylaminopropyl)-3-ethylcarbodiimide hydrochloride (114 mg, 0.596 mmol) in DCM (1 mL) was added. After stirring for 23 h at room temperature, the reaction mixture was purified by flash chromatography using a gradient of $CHCl_3$ to $CHCl_3$ containing 6% Et_2O. Drying of the product in vacuo resulted in the title compound as a white foam (89 mg, 51%). ^{1}H NMR ($CDCl_3$, 400 MHz): δ 7.66 (d, 2H, J = 7.3 Hz); 7.49 (d, 2H, J = 7.3 Hz); 7.30 (t, 2H, J = 7.3 Hz); 7.22 (d, 2H, J = 7.3 Hz); 6.96–6.87 (m, 3H); 6.20 (br s, 1H); 5.38 (br s, 1H); 4.38 (d, 2H J = 6.2 Hz); 4.13 (t, 1H, J = 7.0 Hz); 3.74 (s, 2H); 2.67 (t, 6H, J = 7.5); 2.20 (t, 6H, J = 7.7 Hz). ^{13}C NMR ($CDCl_3$, 50 MHz): δ 167.7; 147.0; 142.2; 139.9; 136.8; 126.4; 125.7; 123.6; 118.6; 101.9; 66.0; 56.2; 45.7; 44.2; 28.4; 26.3. IR (cm^{-1}): ν 3305, 3080, 2910, 1786, 1685, 1524, 1488, 1265, 1178, 1097, 957, 760. MALDI-TOF-MS: calcd $C_{45}H_{30}F_{12}N_2O_9Na^+$: m/z 993.16; found m/z 993.17.

4.4.4. tBoc-aminooxy-PEG-N$_3$

tBoc-aminooxy-OSu (500 mg, 2.4 mmol) was dissolved in DCM (5 mL). To this solution dry DIPEA (1.2 mL, 6.8 mmol) and NH_2-PEG-N_3 (800 mg, 2.3 mmol) were added. After stirring for 22 h at room temperature, the product was purified by a DOWEX MONOSPERE 55 Å anion exchange column (in methanol). Evaporation of the solvent and drying in vacuo resulted in the title compound as a yellow oil (192 mg, 40%). ^{1}H NMR ($CDCl_3$, 400 MHz): δ 7.91 (br s, 1H); 7.75 (br s, 1H); 4.27 (s, 2H); 3.62–3.31 (m, 28H); 1.42 (s, 9H). ^{13}C NMR ($CDCl_3$, 100 MHz): δ 168.7; 156.9; 82.0; 75.4; 70.1; 50.2; 38.5; 27.7. IR (cm^{-1}): ν 2871, 2102, 1660, 1251, 1099, 946, 850, 773. MALDI-TOF-MS: calcd $C_{21}H_{41}N_5O_{10}H^+$: m/z 546.27; found m/z 546.26.

4.4.5. tBoc-aminooxy-PEG-NH$_2$ (5)

tBoc-aminooxy-PEG-N_3 (303 mg, 0.579 mmol) was dissolved in methanol (20 mL) under an inert atmosphere. Pd/C (10% Pd, 60 mg) in methanol (10 mL) followed by H_2. After stirring for 3 h at room temperature the reaction mixture was filtered through a short plug of Celite to remove the Pd/C. Evaporation under reduced pressure yielded the product as a yellow oil (272 mg, 95%) ^{1}H NMR ($CDCl_3$, 400 MHz): δ 7.74 (br s, 1H); 4.27 (s, 2H); 3.57–3.41 (m, 28H); 1.41 (s, 9H). ^{13}C NMR ($CDCl_3$, 100 MHz): δ 169.3; 157.6; 82.3; 70.6; 41.8; 39.0; 28.3. IR (cm^{-1}): ν 3301, 2871, 1725, 1667, 1548, 1458, 1368, 1350, 1285, 1253, 1110, 951, 851. MALDI-TOF-MS: calcd $C_{21}H_{43}N_3O_{10}H^+$: m/z 498.30; found m/z 498.42.

4.4.6. Fmoc-Gly-(tBoc-aminooxy)$_3$ (6)

DIPEA (64 mg, 0.515 mmol) and tBoc-aminooxy-PEG-NH_2 (**5**) (85 mg, 0.170 mol) were dissolved in dry DCM (5 mL). After adding Fmoc-Gly-(TFP)$_3$ (**4**) (50 mg, 0.052 mmol) in DCM (2 mL), the mixture was stirred for 5 h at room temperature. The reaction mixture was diluted with DCM (13 mL), extracted with an aqueous saturated $NaHCO_3$ solution (3 × 25 mL), filtered and dried overnight in vacuo. This resulted in the title compound as a yellow oil (90 mg, 88%). ^{1}H NMR ($CDCl_3$, 400 MHz): δ 8.57 (br s, 3H); 7.88 (br s, 3H); 7.68 (d, 2H, J = 7.0 Hz); 7.55 (d, 2H, J = 7.3 Hz); 7.31 (d, 2H, J = 7.0 Hz); 7.25 (d, 2H, J = 7.7 Hz); 6.75 (br s, 3H); 6.19 (br s, 1H); 4.36 (d, 2H, J = 6.6 Hz); 4.27 (s, 6H); 4.16 (t, 1H, J = 6.7 Hz); 3.72 (d, 2H, J = 5.1 Hz); 3.58–3.22 (m, 84H); 2.14 (t, 6H, J = 7.5 Hz); 1.95 (d, 6H, J = 7.3); 1.40 (s, 27H). ^{13}C NMR ($CDCl_3$, 50 MHz): δ 172.1; 168.3; 156.5; 143.3; 140.1; 127.7; 126.5; 124.2; 120.0; 106.8; 81.2; 69.4; 67.7; 56.9; 46.2; 43.9; 38.3; 37.9; 29.4; 28.7; 27.2. IR (cm^{-1}): ν 3301, 2871, 1721, 1650, 1546, 1452, 1368, 1349, 1280, 1251, 1101, 948, 849, 785, 739, 668. MALDI-TOF-MS: calcd $C_{90}H_{153}N_{11}O_{36}Na^+$: m/z 1988.22; found m/z 1988.03.

4.4.7. NH$_2$-(tBoc-aminooxy)$_3$ (7)

Fmoc-Gly-(tBoc-aminooxy)$_3$ (**6**) (420 mg, 0.229 mmol) was dissolved in 20% v/v piperidine in DCM (15 mL) and stirred for 2.5 h at room temperature. The reaction mixture was diluted with DCM (100 mL), washed with phosphate buffer containing 1 M NaCl pH 5.5 (5 × 100 mL), dried on $MgSO_4$ and filtered. After evaporation of the solvent under reduced pressure, the product was obtained as a yellow oil (385 mg, 95%). ^{1}H NMR ($CDCl_3$, 400 MHz): δ 4.33 (s, 6H); 3.76 (s, 2H); 3.69–3.39 (m, 84H); 2.25 (s, 6H); 2.03

(s, 6H). 1.46 (s, 27H). ^{13}C NMR ($CDCl_3$, 50 MHz): δ 172.5; 168.3; 156.2; 81.2; 74.8 69.2; 53.8; 43.8; 38.6; 37.9; 29.2; 28.7; 27.1. IR (cm^{-1}): ν 3283, 2870, 1723, 1649, 1549, 1505, 1452, 1368, 1349, 1279, 1251, 1099, 933, 783, 737. MALDI-TOF-MS: calcd $C_{75}H_{143}N_{11}O_{34}Na^+$: m/z 1764.97; found m/z 1764.87.

4.4.8. NH_2-(aminooxy)$_3$ (8)

To a mixture of cooled TFA containing 2.5% v/v water and triisopropylsilane (30 mL) was added NH_2-(tBoc-aminooxy)$_3$ (**9**) (330 mg, 0.189 mmol). After stirring for 1 h at 0 °C the solvents where evaporated under reduced pressure. The resulting mixture was dissolved in water (100 mL) and washed with diethyl ether (4 × 100 mL). The solvent volume was reduced by freeze drying and the resulting solution was purified by preparative RP-HPLC using a gradient of 5–35% CH_3CN in water (both containing 0.1% TFA) over 60 min. Freeze drying resulted in a viscous, colorless oil (90 mg, 33%). ^{1}H NMR (methanol-d_4, 400 MHz): δ 4.37 (s, 6H); 3.75 (s, 2H); 3.68–3.36 (m, 84H); 2.22 (s, 6H); 2.03 (s, 6H). ESI-MS: calcd $C_{60}H_{119}N_{11}O_{28}H^+$: m/z 1443.66; found m/z 1443.6.

4.4.9. S-(GPO)$_5$-NH_2

Synthesis of the peptide Ser-Gly-Pro-Hyp-Gly-Pro-Hyp-Gly-Pro-Hyp-Gly-Pro-Hyp-Gly-Pro-Hyp was performed on an automated peptide synthesizer (Prelude, Protein technologies) following the standard Fmoc peptide synthesis protocol on 50 μmol scale. Each amino acid was allowed to couple two times 20 min. The peptide was cleaved from the resin using a mixture of TFA/H_2O/TIS/EDT (v/v/v/v 50:1:1:1) (5.3 mL). After stirring for 2 h at room temperature the mixture was filtered and cold diethyl ether (50 mL) was added. The mixture was kept for 2 h at −30 °C. The precipitate formed after centrifugation was dissolved in water and lyophilized. Purification was performed using preparative RP-HPLC using a gradient of 5–22% CH_3CN in water (both containing 0.1% TFA) over 36 min. Freeze drying resulted in the pure peptide (56%). ESI-MS: calcd $C_{63}H_{94}N_{17}O_{22}H^+$: m/z 1440.7; found m/z 1440.5.

4.4.10. Glyoxyl-(GPO)$_5$-NH_2 (9)

S-(GPO)$_5$-NH_2 (13 mg, 0.009 mmol) was dissolved in 0.01 M sodium phosphate buffer pH 7.0 (2 mL) and $NaIO_4$ (2.9 mg, 0014 mmol) was added. The mixture was allowed to react at room temperature for 15 min and was subsequently purified by preparative RP-HPLC using a gradient of 2–18% CH_3CN in water (both containing 0.1% TFA) over 41 min. This resulted in the title compound with a yield of 78%. ESI-MS: calcd $C_{62}H_{88}N_{16}O_{22}H^+$: m/z 1409.6; found m/z 1409.2.

4.4.11. Collagen mimic, NH_2-((GPO)$_5$)$_3$ (10)

NH_2-(aminooxy)$_3$ (**8**) (2.2 mg, 0.002 mmol) and glyoxyl-(GPO)$_5$-NH_2 (7.1 mg, 0.006 mmol) were dissolved in 0.01 M sodium phosphate buffer pH 7.0 (600 μL) and allowed to react overnight at room temperature. Purification was performed by preparative RP-HPLC using a gradient of 5–35% CH_3CN in water (both containing 0.1% TFA) over 35 min. This resulted in the pure title compound with a yield of ∼10%. ESI-MS: calcd $C_{246}H_{377}N_{59}O_{91}$: m/z 5616.97; found m/z 5615.24.

4.5. SPR measurements

SPR measurements were performed on a BIAcore T100 (GE Healthcare). Human collagen type I and the collagen mimic were immobilized on CM5 chips using standard EDC/NHS protocols. All binding experiments were performed at 25 °C at a flow rate of 5 μL/min. The affinity measurement depicted in Figure 4C was performed at a flow rate of 10 μL/min. Binding experiments with human collagen type I were performed using HBS containing 1 mg/mL from bovine serum albumin (BSA) as a running buffer. Binding experiments with the collagen mimic were performed using HBS-EP (HBS containing 3 mM EDTA and 0.05% v/v Surfactant P20) as a running buffer. To prevent hydrolysis of the C-terminal thioester CNA35-MESNA was always stored at pH 6 and only diluted to HBS buffer just before the binding experiment. Regeneration of the chips was performed using glycine-HCl (pH 1.5, 30 s). After regeneration to remove all bound probe, the chip was reused again to measure other probes under the same surface conditions. Non-specific binding and buffer effects were taken into account by subtracting the simultaneous response from a reference surface only functionalized with ethanolamine.

4.6. Tissue experiments

Proteins were buffer exchanged to $NaHCO_3$ buffer (0.1 M, pH 8.5) and subsequently labeled with Oregon Green 488 (OG-488) by adding a 10-fold molar excess of Oregon Green 488 succinimidyl ester from a stock solution in DMF (20 mM) at a protein concentration of ∼100 μM according to the protocol for amine-reactive dyes (Molecular Probes, Invitrogen). After overnight incubation at room temperature, unreacted dye molecules were removed and buffer was exchanged to HBS by repeated concentration and dilution using an Amicon Ultra-4 centrifugal filter tube with a 10 kDa cut-off membrane. The concentration of protein and labeling efficiency was determined by measuring the absorbance at 280 nm and 496 nm, respectively, using a NanoDrop ND-1000 spectrophotometer (ε_{280nm} = 29,910 M^{-1} cm^{-1}, ε_{496nm} = 70,000 M^{-1} cm^{-1} and a correction factor for the 280 nm signal of 0.12).

Frozen sections of rat intestinal tissue on Starfrost microscope slides were defrosted. OG-488 labeled (CNA35)$_{3-4}$, (CNA35 (Y175K))$_{3-4}$ and their monovalent analogues were diluted in HBS containing 1 mg/mL BSA to a final protein concentration of 0.5 μM. The sections of rat intestinal tissue were incubated with 1.35 mL of the protein solutions overnight at room temperature protected from light. After overnight incubation, the slides were washed three times for 5 min in HBS. After washing, the sections were mounted using FluorSave (VWR) and covered with a glass coverslip. Images were obtained using an inverted Zeiss Axiovert 200 microscope coupled to an LSM 510 Meta (Carl Zeiss, Germany) laser scanning microscope with a 20× objective. Excitation was performed using an argon laser (488 nm).

Acknowledgments

The authors thank Patricia Dankers for providing the sections of rat intestinal tissue and useful discussions. This work was supported by a grant from NWO (VIDI 700 56.428).

Supplementary data

Supplementary data associated with this article can be found, in the online version, at doi:10.1016/j.bmc.2010.07.058.

References and notes

1. Allen, T. M.; Cullis, P. R. *Science* **2004**, *303*, 1818.
2. Artemov, D. *J. Cell. Biochem.* **2003**, *90*, 518.
3. Gu, F. X.; Karnik, R.; Wang, A. Z.; Alexis, F.; Levy-Nissenbaum, E.; Hong, S.; Langer, R. S.; Farokhzad, O. C. *Nano Today* **2007**, *2*, 14.
4. Morawski, A. M.; Lanza, G. A.; Wickline, S. A. *Curr. Opin. Biotechnol.* **2005**, *16*, 89.
5. Martos, V.; Castreno, P.; Valero, J.; de Mendoza, J. *Curr. Opin. Chem. Biol.* **2008**, *12*, 698.
6. Kiessling, L. L.; Gestwicki, J. E.; Strong, L. E. *Angew. Chem., Int. Ed.* **2006**, *45*, 2348.
7. Mammen, M.; Choi, S. K.; Whitesides, G. M. *Angew. Chem., Int. Ed.* **1998**, *37*, 2755.
8. Andre, T.; Reichel, A.; Wiesmuller, K. H.; Tampe, R.; Piehler, J.; Brock, R. *ChemBioChem* **2009**, *10*, 1878.
9. Huskens, J. *Curr. Opin. Chem. Biol.* **2006**, *10*, 537.

10. Huskens, J.; Mulder, A.; Auletta, T.; Nijhuis, C. A.; Ludden, M. J. W.; Reinhoudt, D. N. *J. Am. Chem. Soc.* **2004**, *126*, 6784.
11. Munoz, E. M.; Correa, J.; Fernandez-Megia, E.; Riguera, R. *J. Am. Chem. Soc.* **2009**, *131*, 17765.
12. Kluger, R.; Zhang, J. *J. Am. Chem. Soc.* **2003**, *125*, 6070.
13. Lempens, E. H. M.; Van Baal, I.; Van Dongen, J. L. J.; Hackeng, T. M.; Merkx, M.; Meijer, E. W. *Chemistry* **2009**, *15*, 8760.
14. Reulen, S. W. A.; Brusselaars, W. W. T.; Langereis, S.; Mulder, W. J. M.; Breurken, M.; Merkx, M. *Bioconjugate Chem.* **2007**, *18*, 590.
15. Van Baal, I.; Malda, H.; Synowsky, S. A.; Van Dongen, J. L. J.; Hackeng, T. M.; Merkx, M.; Meijer, E. W. *Angew. Chem., Int. Ed.* **2005**, *44*, 5052.
16. Zhou, M.; Bentley, D.; Ghosh, I. *J. Am. Chem. Soc.* **2004**, *126*, 734.
17. Arroyo, L. H.; Lee, R. T. *Cardiovasc. Res.* **1999**, *41*, 369.
18. Katsuda, S.; Kaji, T. *J. Atheroscler. Thromb.* **2003**, *10*, 267.
19. Vakonakis, I.; Campbell, I. D. *Curr. Opin. Cell Biol.* **2007**, *19*, 578.
20. Weisman, H. F.; Healy, B. *Progr. Cardiovasc. Dis.* **1987**, *30*, 73.
21. Gelse, K.; Pöschl, E.; Aigner, T. *Adv. Drug Deliv. Rev.* **2003**, *55*, 1531.
22. Brodsky, B.; Ramshaw, J. A. M. *Matrix Biol.* **1997**, *15*, 545.
23. Cejas, M. A.; Chen, C.; Kinney, W. A.; Maryanoff, B. E. *Bioconjugate Chem.* **2007**, *18*, 1025.
24. Santoro, S. A.; Cunningham, L. W. *J. Clin. Invest.* **1977**, *60*, 1054.
25. Reulen, S. W. A.; Dankers, P. Y. W.; Bomans, P. H. H.; Meijer, E. W.; Merkx, M. *J. Am. Chem. Soc.* **2009**, *131*, 7304.
26. Zong, Y.; Xu, Y.; Liang, X.; Keene, D. R.; Höök, A.; Gurusiddappa, S.; Höök, M.; Narayana, S. V. L. *EMBO J.* **2005**, *24*, 4224.
27. Boerboom, R. A.; Krahn, K. N.; Megens, R. T. A.; van Zandvoort, M. A. M. J.; Merkx, M.; Bouten, C. V. C. *J. Struct. Biol.* **2007**, *159*, 392.
28. Megens, R. T. A.; Oude Egbrink, M. G. A.; Cleutjens, J. P. M.; Kuijpers, M. J. E.; Schiffers, P. H. M.; Merkx, M.; Slaaf, D. W.; Van Zandvoort, M. A. M. J. *Mol. Imaging* **2007**, *6*, 247.
29. Symersky, J.; Patti, J. M.; Carson, M.; House-Pompeo, K.; Teale, M.; Moore, D.; Jin, L.; Schneider, A.; Delucas, L. J.; Höök, M.; Narayana, S. V. L. *Nat. Struct. Biol.* **1997**, *4*, 833.
30. Peters, D.; Kastantin, M.; Kotamraju, V. R.; Karmali, P. P.; Gujraty, K.; Tirrell, M.; Ruoslahti, E. *Proc. Natl. Acad. Sci. USA* **2009**, *106*, 9815.
31. Reulen, S. W. A.; Merkx, M. *Bioconjugate Chem.* **2010**, *21*, 860.
32. Helms, B. A.; Reulen, S. W. A.; Nijhuis, S.; de Graaf-Heuvelmans, P. T. H. M.; Merkx, M.; Meijer, E. W. *J. Am. Chem. Soc.* **2009**, *131*, 11683.
33. Lempens, E. H. M.; Helms, B. A.; Bayles, A. R.; Merkx, M.; Meijer, E. W. *Eur. J. Org. Chem.* **2010**, *2010*, 111.
34. Johnson, E. C. B.; Kent, S. B. H. *J. Am. Chem. Soc.* **2006**, *128*, 6640.
35. Krahn, K. N.; Bouten, C. V. C.; Van Tuijl, S.; Van Zandvoort, M. A. M. J.; Merkx, M. *Anal. Biochem.* **2006**, *350*, 177.
36. Patti, J. M.; Boles, J. O.; Höök, M. *Biochemistry* **1993**, *32*, 11428.
37. Rich, R. L.; Deivanayagam, C. C. S.; Owens, R. T.; Carson, M.; Hook, A.; Moore, D.; Yang, V. W. C.; Narayana, S. V. L.; Höök, M. *J. Biol. Chem.* **1999**, *274*, 24906.
38. Feng, Y.; Melacini, G.; Taulane, J. P.; Goodman, M. *J. Am. Chem. Soc.* **1996**, *118*, 10351.
39. Mingels, A. M. A.; van Dongen, J. L. J.; Merkx, M. *J. Chromatogr., B* **2008**, *863*, 293.